JOC Article

Importance of Entropy in the Diastereoselectivity of 5-Substituted 2-Methyladamant-2-yl Cations

Antonello Filippi,[†] Neil A. Trout,[‡] Patrick Brunelle,[§] William Adcock,*[,‡] Ted S. Sorensen,*[,§] and Maurizio Speranza*[,†]

Dipartimento di Studi di Chimica e Tecnologia delle Sostanze Biologicamente Attive, Università di Roma "La Sapienza", 00185 Roma, Italy, the School of Chemistry, Physics, and Earth Sciences, The Flinders University of South Australia, Adelaide, Australia 5001, and the Department of Chemistry, University of Calgary, Calgary, Alberta T2N 1N4, Canada

maurizio.speranza@uniroma1.it

Received March 31, 2004

The diastereofacial selectivity of 2-methyl-5-X-adamant-2-yl cations $\mathbf{I_X}$ (X = CN, Cl, Br, CH_3O, $COOCH_3$, C_6H_5, CH_3, and $(CH_3)_3Sn$) toward methanol has been investigated in the gas phase at 750 Torr and in the 40−120 °C temperature range and compared with that of $\mathbf{I_F}$ (X = F) and $\mathbf{I_{Si}}$ (X = $(CH_3)_3Si$) measured previously under similar conditions. Detailed analysis of the energy surface of the $\mathbf{I_{Me}}$ (X = CH_3) ion reveals that the activation barrier of its *syn* addition to methanol is significantly lower than that of the *anti* attack. In the 40−100 °C range, such a difference is strongly reduced by adverse entropic factors which are large enough to invert the $\mathbf{I_{Me}}$ diastereoselectivity from *syn* to *anti* at $T > 69$ °C. The behavior of $\mathbf{I_{Me}}$ diverges markedly from that of $\mathbf{I_F}$ and $\mathbf{I_{Si}}$. Large adverse entropic factors account for the predominant *syn* diastereoselectivity observed in the reaction with $\mathbf{I_F}$ (X = F), notwithstanding the *anti* enthalpy barrier is lower than the *syn* one. Adverse entropy plays a minor role in the reaction with $\mathbf{I_{Si}}$ (X = $(CH_3)_3Si$) which instead exhibits a preferred *anti* diastereoselectivity governed by the activation enthalpies. Depending on the electronic properties of X, the kinetic behavior of the other $\mathbf{I_X}$ ions obeys one of the above models. The gas-phase diastereoselectivity of $\mathbf{I_X}$ ions responds to a subtle interplay between the σ-hyperconjugative/electrostatic effects of the X substituent and the activation entropy terms. σ-Hyperconjugation/field effects determine the pyramidal structure and the relative stability of the *syn* and *anti* conformers of $\mathbf{I_X}$ as well as the relative stability of their addition transition structures and their position along the reaction coordinate. The diastereoselectivity of $\mathbf{I_X}$ in the gas phase is compared with that measured in solution and with theoretical predictions.

Introduction

Disentanglement of the factors determining facial selectivity in sterically unbiased substrates, such as the 2-methyl-5-X-adamant-2-yl cation $\mathbf{I_X}$ (Chart 1), continues to be a challenging problem despite the large body of experimental and theoretical evidence and the development of novel methodologies of investigation.[1] Nucleophilic capture of $\mathbf{I_X}$ by ionic and neutral nucleophiles provides some of the most conspicuous examples of electronically induced diastereoselectivity. For example, a powerful σ-electron-withdrawing group, such as X = F, can lead to a nucleophilic capture ratio (Z/E) in excess of 9:1.[1a,b] *Syn* (or *zu*) approach of the nucleophile is favored by these groups but, with σ-electron donors (e.g., $SiMe_3$), diametrically opposite stereochemistry (*anti* or *en*) is induced. The π-facial selectivity has been ascribed to predominantly differential hyperconjugative effects induced by the substituent at C5 on the relative stability

CHART 1

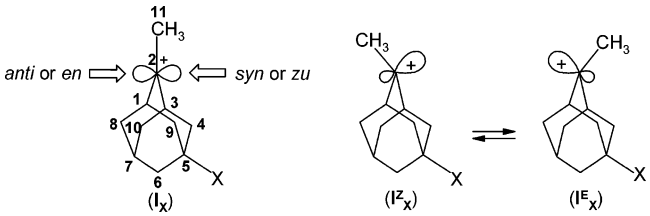

of rapidly equilibrating pyramidalized *syn* and *anti* epimeric ions (free or intimate ion-pairs, $\mathbf{I^Z_X} \leftrightarrows \mathbf{I^E_X}$; Chart 1) prior to nucleophilic capture.[1−5]

Under conditions where nucleophilic trapping of the epimeric cations is essentially diffusion controlled,[6] then facial selectivity will be entirely controlled by the relative concentration of the epimeric ions rather than their

* To whom correspondence should be addressed.
[†] Università di Roma "La Sapienza".
[‡] The Flinders University of South Australia.
[§] University of Calgary.

(1) For reviews on this topic, see the special issue: *Chem. Rev.* **1999**, *99* (5): (a) Kaselj, M.; Chung, W.-S.; le Noble, W. J. *Chem. Rev.* **1999**, *99* (5), 1387. (b) Adcock, W.; Trout, N. A. *Chem. Rev.* **1999**, *99* (5), 1415.

(2) Adcock, W.; Cotton, J.; Trout, N. A. *J. Org. Chem.* **1994**, *59*, 1867.
(3) Herrmann, R.; Kirmse, W. *Liebigs Ann.* **1995**, 699.
(4) Adcock, W.; Head, N. J.; Lokan, N. R.; Trout, N. A. *J. Org. Chem.* **1997**, *62*, 6177.
(5) Rauk, A.; Sorensen, T. S.; Schleyer, P. von R. *J. Chem. Soc., Perkin Trans. 2* **2001**, 869.
(6) Carbocations which are not highly stabilized are known to be quenched by nucleophiles at the diffusional rate. See: (a) McCelland, R. A. *Tetrahedron* **1996**, *52*, 6823. (b) Richard, J. P.; Amyes, T. L.; Toteva, M. M. *Acc. Chem. Res.* **2001**, *34*, 981 and references therein.

10.1021/jo049481l CCC: $27.50
Published on Web 07/17/2004

relative reactivity.[1b] In circumstances where the latter situation holds, the hyperconjugative mode differentiates the energies of the diastereomeric transition states (Cieplak's model of kinetic diastereoselectivity).[1] Since hyperconjugation is promoted by enhanced electron demand, differential stabilization of the epimeric cations should be greater than that of the diastereomeric transition states. Hence, stereoselectivity should be most pronounced for rapid (diffusion controlled) nucleophilic capture of $\mathbf{I_X}$**.** The opposite diastereoselectivity exhibited by $\mathbf{I_X}$ with X = $(CH_3)_3Si$ and $(CH_3)_3C$,[2,4] two substituents with virtually no electrostatic field influence ($\sigma_F \sim 0$)[1b] but opposite σ-electron-donor/withdrawing character, exemplifies the importance of extended hyperconjugation[1b,7] as a control factor.

Despite this apparently unequivocal model, several important facets of the problem remain obscure. A first question concerns the electrostatic effects which may be an important component of the electronic influence of electron-withdrawing polar substituents ($\sigma_F > 0.15$).[1b,2] This is apparent from the excellent correlation between log *Z*/*E* values for hydrochlorination in CH_2Cl_2 of a series of 2-methylene-5-(para-substituted(S)phenyl)adamantanes and $\Delta\sigma_F$.[1b,2] Calculated diastereoselectivities (log $Z/E = \rho_{FS}\sigma_F$) of $\mathbf{I_X}$, based on the polar susceptibility parameter (ρ_{FS}) derived from the aforementioned correlation, agree quite well with the observed selectivities for most of the σ-electron-withdrawing groups ($\sigma_F > 0.15$).[1b,2] Other evidence is available for an intimate combination of electrostatic field and hyperconjugative effects in controlling facial selectivity in $\mathbf{I_X}$.[8] This is not particularly surprising given that orbital energy gap[9] considerations suggest that the dominant perturbation between the p-orbital of the C^+ center and the *anti*-vicinal C−C bonds in the $\mathbf{I^E_X}$ cation (or *anti*-configurated transition state) ensures that the hyperconjugating influence of the substituent ($\sigma_{CC}-\sigma_{CX}$*) has only a minor effect on the intrinsic donor capacity of the proximate C−C bonds. Thus, the preferential *syn*-face selectivity induced in $\mathbf{I_X}$ by the electrostatic field of relatively strong σ-electron-withdrawing groups is a consequence of Coulombic forces of repulsion being minimized by delocalizing the positive charge away from the polarity of the acceptor substituents (the partial formal charge at C5 being paramount). Obviously, in this regard, $\mathbf{I^Z_X}$ is the favored invertomer.

A second question regards the often unpredictable effects of solvent, counterion, and temperature.[2−5] Indeed, precise evaluation of $\mathbf{I_X}$ diastereoselectivity in solution is conditioned by the experimental procedures adopted for generating the cation, and therefore, it is susceptible to the influence of the dielectric medium and of the counterion on the transmission of the effects of the polar X substituent to the $\mathbf{I_X}$ reaction center. To single out these effects from intrinsic electronic factors, we recently carried out an exhaustive kinetic analysis of the gas-phase addition of methanol to two representative $\mathbf{I_X}$ ions with X = F ($\mathbf{I_F}$); $(CH_3)_3Si$ ($\mathbf{I_{Si}}$), i.e., substituents with opposite electronic properties.[10] Their diastereoselectivity was found to be determined not only by the relative stability of the corresponding *anti* and *syn* transition structures but also by adverse activation entropies associated with their position along the relevant reaction coordinate.

SCHEME 1

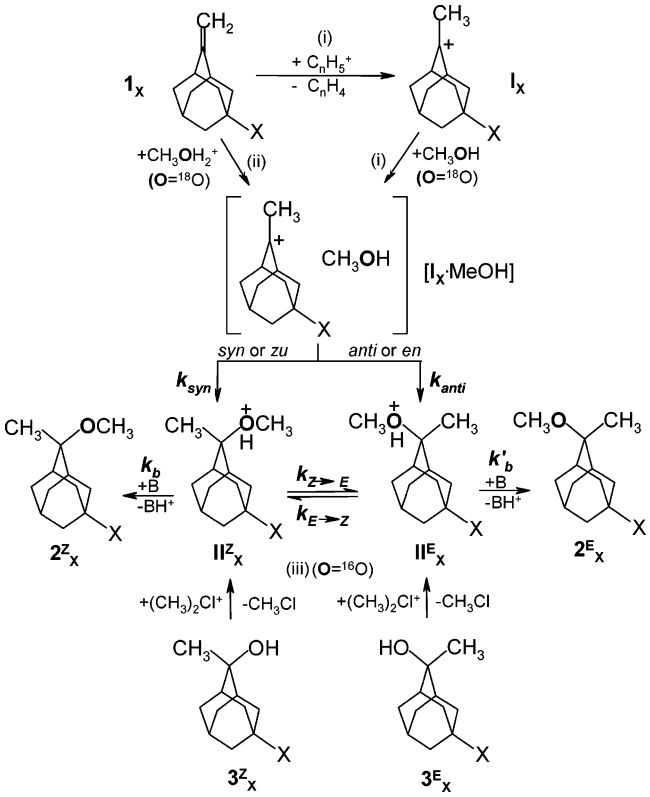

In this paper, the study has been extended to a number of $\mathbf{I_X}$ cations containing various σ-electron-withdrawing (X = CN, Cl, Br, CH_3O, $COOCH_3$, C_6H_5, and CH_3) and -donor (X = $(CH_3)_3Sn$) substituents.[11] In particular, we weighed the contribution of entropic factors on the gas-phase facial selectivity of the $\mathbf{I_X}$ with X = CH_3 ($\mathbf{I_{Me}}$), namely a substituent with electronic properties between those of F and $(CH_3)_3Si$.[10] Furthermore, from the comparison of the gas-phase kinetic results with those obtained in related reactions in solution, it is hoped to evaluate the effects of solvation and ion pairing on the intrinsic factors governing $\mathbf{I_X}$ facial selectivity.

The experimental methodology used has been described in detail elsewhere.[10] Briefly, the $\mathbf{I_X}$ cation is generated in the gas phase by two different procedures (Scheme 1): (i) by protonation of the corresponding 2-methylene-5-X-adamantane $\mathbf{1_X}$ with $C_nH_5^+$ (n = 1, 2) ions, formed from γ-irradiation (^{60}Co γ-rays, T = 40−120 °C) of gaseous CH_4 mixtures. Protonation takes place in the presence of traces of a nucleophile ($CH_3{}^{18}OH$, ^{18}O-content = 95%), a radical scavenger (O_2), and a power-

(7) (a) Adcock, W.; Trout, N. A. *J. Org. Chem.* **1991**, *56*, 3229. (b) Adcock, W.; Trout, N. A. *Magn. Reson. Chem.* **1998**, *36*, 181.

(8) The situation is somewhat akin to the mesomeric-field effect in aromatic systems. See: (a) Dewar, M. J. S.; Golden, R.; Harris, J. M. *J. Am. Chem. Soc.* **1971**, *93*, 4187 and references therein. (b) Adcock, W.; Bettess, P. D.; Rizvi, S. Q. A. *Aust. J. Chem.* **1970**, *23*, 1921 and references therein.

(9) (a) Dewar, M. J. S.; Dougherty, R. C. *The PMO Theory of Organic Chemistry*; Plenum Press: New York, 1975. (b) Epiotis, N. D.; Cherry, W. R.; Shaik, S.; Yates, R. L.; Bernardi, F. *Top. Curr. Chem.* **1977**, *70*, 1. (c) Alabugin, I. V.; Zeidan, T. A. *J. Am. Chem. Soc.* **2002**, *124*, 3175.

(10) Filippi, A.; Trout, N. A.; Brunelle, P.; Adcock, W.; Sorensen, T. S.; Speranza, M. *J. Am. Chem. Soc.* **2001**, *123*, 6396.

(11) Direct investigation of the diastereoselectivity of $\mathbf{I_X}$ (X = $(CH_3)_3$-Sn) in solution is prevented by the marked propensity of the tin species to undergo fragmentation and, as well, its fragility under strong acidic or electrophilic conditions (refs 1b and 2).

ful base B ($(C_2H_5)_3N$) (the *extracomplex* path i); (ii) by protonation of $\mathbf{1_X}$ with $CH_3{}^{18}OH_2{}^+$ ions, formed by methylation of added $H_2{}^{18}O$ (^{18}O-content > 97%) with $(CH_3)_2F^+$ ions. These latter ions are obtained by γ-irradiating gaseous CH_3F mixtures. By this procedure, the $CH_3{}^{18}OH_2{}^+$ ions are formed in the complete absence of neutral $CH_3{}^{18}OH$ molecules.[12] Under such conditions, the ^{18}O-labeled ethereal products $\mathbf{2^Z_X}$ and $\mathbf{2^E_X}$ must necessarily arise from the addition of the incipient $CH_3{}^{18}OH$ molecule on the putative $\mathbf{I_X}$ cation within their [$\mathbf{I_X}$·$CH_3{}^{18}OH$] complex (the *intracomplex* path ii). Procedures i and ii use inert bulk gas (CH_4 and CH_3F, respectively) at pressures high enough (750 Torr) to ensure the complete thermalization of all the active species involved.

The potential energy profile of the gas-phase addition of methanol on I_{Me} has been determined by measuring the extent of $\mathbf{II^E_{Me}} \leftrightarrows \mathbf{II^Z_{Me}}$ epimerization ($k_{E\rightarrow Z}$ vs $k_{Z\rightarrow E}$ in Scheme 1) prior to neutralization (k_b and k'_b in Scheme 1). As pointed out elsewhere,[10] the gaseous mixtures used for this purpose were identical to those used in procedure ii except for the bulk gas, CH_3Cl instead of CH_3F (path iii of Scheme 1).[13]

Experimental Section

Materials. Methane, methyl fluoride, methyl chloride, and oxygen were high-purity gases obtained from commercial sources and used without further purification. Commercial sources provided $H_2{}^{18}O$ (^{18}O-content > 97%), $CH_3{}^{18}OH$ (^{18}O-content = 95%), and $(C_2H_5)_3N$ as well.

5-X-adamantan-2-ones (X = Cl, Br, $COOCH_3$, CH_3O, C_6H_5, CH_3, and $(CH_3)_3Sn$) were prepared according to previously described procedures.[2,7a] 5-CN-adamantan-2-one was prepared by treating 5-Br-adamantan-2-one with dry powdered CuCN in pyridine as described by Vogel[14] for the synthesis of 1-naphthonitrile from the corresponding bromide. This route proved more convenient than that previously reported.[2] 2-Methylene-5-X-adamantanes $\mathbf{1_X}$ (X = CN, Cl, Br, $COOCH_3$, CH_3O, C_6H_5, CH_3, and $(CH_3)_3Sn$) were synthesized from the corresponding 5-X-adamantan-2-ones according to previously described procedures.[2,7a]

Biased *E*/*Z* mixtures of 2-methyl-5-X-2-adamantanols ($\mathbf{3^E_X}$/$\mathbf{3^Z_X}$) were obtained as previously described by methylation (MeLi/H_2O) of the corresponding ketones.[2] Except for the trimethylstannyl derivatives, all the *E*/*Z* mixtures of 2-methyl-2-methoxy-5-X-adamantanes ($\mathbf{2^E_X}$/$\mathbf{2^Z_X}$) were obtained from the corresponding tertiary alcohols $\mathbf{3^E_X}$/$\mathbf{3^Z_X}$ by treatment with NaH/MeI as previously described for the preparation of (*E*)-2-methyl-2-methoxy-5-$(CH_3)_3$Si-adamantane.[10] The tin−ether mixture was obtained by trimethylstannylation of the corresponding bromo ether mixture in exactly the same manner as previously described for the synthesis of 2-methylene-5-$(CH_3)_3$-Sn-adamantane.[2] A more biased mixture (*E*/*Z* = 60/40) of the 5-methyl tertiary ethers was obtained by the same procedure used for the preparation of 2-methyl-2-methoxy-adamantane,[10] i.e., by methanolysis (MeOH/$AgNO_3$) of the corresponding tertiary chloride mixture (*E*/*Z* = 60/40) obtained from the hydrochlorination of 2-methylene-5-methyladamantane ($\mathbf{1_{Me}}$).[2] Hydrolysis (THF/H_2O/$AgNO_3$) of the chloride mixture gave a similarly biased mixture (*E*/*Z* = 60/40) of the 5-methyl tertiary alcohols. The tertiary alcohol mixture ($\mathbf{3^E_{Me}}$/$\mathbf{3^Z_{Me}}$) was first separated by chromatography on alumina (dry ether as eluent) as described in the literature.[15] The impure epimers were then purified by preparative GLC on a 10% Silicone OV17 on Chromosorb Wax 80−100 mesh, 2 m long, 4.5 mm i.d., stainless steel column, operated at 50 < *T* <100 °C, 10 °C min^{-1}. Pure epimeric ethers ($\mathbf{2^E_{Me}}$ and $\mathbf{2^Z_{Me}}$) were separated from their synthetic mixture by preparative GLC as described above for $\mathbf{3^E_{Me}}$ and $\mathbf{3^Z_{Me}}$. ^{13}C NMR chemical shift data of the tertiary ethers, which were assigned largely by additivity methodology,[16] are contained in the Supporting Information together with their calculated spectra (Tables S2−S5).

Procedure. The gaseous mixtures were prepared as described previously.[10] In brief, the starting $\mathbf{1_X}$ adamantane, the labeled nucleophile (either $H_2{}^{18}O$ (^{18}O-content > 97%) or $CH_3{}^{18}OH$ (^{18}O-content = 95%)), the thermal radical scavenger O_2, and the base B = $(C_2H_5)_3N$ were introduced into carefully outgassed 130 mL Pyrex bulbs, filled up with the bulk gas (CH_3Y; Y = H, F, or Cl (750 Torr)). The sealed bulbs were submitted to irradiation at a constant temperature ranging from 40 to 120 °C in a ^{60}Co source (dose: 2×10^4 Gy; dose rate: 1×10^4 Gy h^{-1}, determined with a neopentane dosimeter). Control experiments, carried out at doses ranging from 1×10^4 to 1×10^5 Gy, showed that the relative yields of products are largely independent of the dose. The radiolytic products were analyzed by GLC on: (i) a MEGADEX DACT-BS-*β* (30% 2,3-di-*O*-acetyl-6-*O*-*tert*-butyldimethylsilyl-*β*-cyclodextrin in OV 1701; 25 m long, 0.25 mm i.d., d_f: 0.25 μm) fused silica column, at 60 < *T* < 170 °C, 5 °C min^{-1}; (ii) a MEGADEX 5 (30% 2,3-di-*O*-methyl-6-*O*-pentyl-*β*-cyclodextrin in OV 1701; 25 m long, 0.25 mm i.d., d_f: 0.25 μm) fused silica column operated at 100 < *T* < 165 °C, 5 °C min^{-1}; (iii) a SUPELCO NUKOL (30 m long, 0.25 mm i.d., 0.25 μm) fused silica column operated at 120 < *T* < 170 °C, 10 °C min^{-1}. The products were identified by comparison of their retention volumes with those of authentic standard compounds and their identity confirmed by GLC−MS. Their yields were determined from the areas of the corresponding eluted peaks, using benzyl alcohol, as the internal standard, and individual calibration factors to correct for the detector response. Blank experiments were carried out to exclude the occurrence of thermal decomposition and isomerization of the starting substrates as well as the epimerisation of their ethereal products within the temperature range investigated.

The extent of ^{18}O incorporation into the radiolytic products was determined by GLC−MS, setting the mass analyzer in the selected ion mode (SIM). The ion fragments ^{16}O-[M − CH_3]$^+$ and ^{18}O-[M − CH_3]$^+$ were monitored to analyze all the epimeric $\mathbf{2^E_X}$ and $\mathbf{2^Z_X}$ ethers, except $\mathbf{2^E_{Sn}}$ and $\mathbf{2^Z_{Sn}}$ which were analyzed by monitoring their ^{16}O-[M − $Sn(CH_3)_3$]$^+$ and ^{18}O-[M − $Sn(CH_3)_3$]$^+$ fragments.

Computational Details. Quantum chemical calculations were performed on PC-based computers and the Linux operating system, using the A7 version of the suite of programs in GAUSSIAN 98.[17] The 6-31G* basis set was employed using the B3LYP hybrid density functional procedure.[18] At the same level of theory, frequency calculations were performed for all the optimized structures to ascertain their minimum or transition state nature. Thermal contribution to enthalpy at 298 K and 1 atm, which include the effects of translation, rotation and vibration, was evaluated by classical statistical thermodynamics within the approximation of ideal gas, rigid

(12) Blint, R. J.; McMahon, T. B.; Beauchamp, J. L. *J. Am. Chem. Soc.* **1974**, *96*, 1269.
(13) Speranza, M.; Troiani, A. *J. Org. Chem.* **1998**, *63*, 1020.
(14) Vogel, A. I. *Practical Organic Chemistry*; Longmans: London, 1978; pp 846−847.
(15) Bone, J. A.; Pritt, J. R.; Whiting, M. C. *J. Chem. Soc., Perkin Trans. 1* **1972**, 2644.
(16) Srivastava, S.; Cheung, C. K.; le Noble, W. *J. Magn. Reson. Chem.* **1985**, *23*, 232.
(17) Frish, M. J.; Trucks, G. W.; Schlegel, H. B.; Gill, P. M. W.; Johnson, B. G.; Robb, M. A.; Cheeseman, J. R.; Keith, T. A.; Petersson, G. A.; Montgomery, J. A.; Raghavachari, K.; Al-Laham, M. A.; Zakrzewski, V. G.; Ortiz, J. V.; Foresman, J. B.; Cioslowski, J.; Stefanov, B. B.; Nanayakkara, A.; Challacombe, M.; Peng, C. Y.; Ayala, P. Y.; Chen, W.; Wong, M. W.; Andres, J. L.; Repogle, E. S.; Gomperts, R.; Martin, R. L.; Fox, D. J.; Binkley, J. S.; Defrees, D. J.; Baker, J.; Stewart, J. P.; Head-Gordon, M.; Gonzales, C.; Pople, J. A. *Gaussian 98*, Revision C.2; Gaussian, Inc.: Pittsburgh, PA, 1995.
(18) (a) Becke, A. D. *J. Chem. Phys.* **1993**, *98*, 1372, 5648. (b) Lee, C.; Yang, W.; Parr, R. G. *Phys. Rev. B* **1988**, *37*, 785.

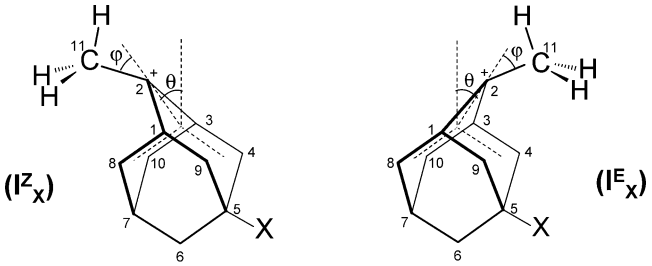

System	C1-C8 (Å)	C1-C9 (Å)	θ (degrees)	φ (degrees)
I^Z_H	1.607	1.555	11.91	4.82
I^Z_{CN}	1.609	1.548	13.87	6.04
I^Z_{Br}	1.609	1.557	12.59	5.21
I^Z_{Cl}	1.609	1.552	13.95	5.99
I^Z_{OMe}	1.609	1.545	14.14	5.93
I^Z_F	1.612	1.547	14.56	6.21
I^Z_{COOMe}	1.607	1.552	12.86	5.46
I^E_{COOMe}	1.557	1.600	10.63	4.19
I^Z_{Me}	1.601	1.558	12.35	4.92
I^E_{Me}	1.554	1.605	11.15	4.44
I^Z_{Ph}	1.606	1.552	12.70	5.00
I^E_{Ph}	1.554	1.599	11.90	5.11
I^E_{Si}	1.551	1.632	10.16	8.15
I^E_{Ge}	1.552	1.636	12.71	6.89
I^E_{Sn}	1.550	1.653	12.99	7.82

FIGURE 1. B3LYP/6-31G*-optimized geometries of 2-methyl-5-X-2-adamantyl cation $\mathbf{I_X}$. Bond distances C1−C8═C3−C10 and C1−C9═C3−C4. Angle θ is defined as the deviation of the C1−C2−C3 plane from the bisector of the 8−10, 1−3, 9−4 midpoint lines. Angle φ is defined as the C2−C11 bond deviation from the C1−C2−C3 plane in each case.

rotor and harmonic oscillator behavior and using the recommended scale factor (0.98) for frequencies and zero-point energy correction.[19]

Results

Theoretical Calculations. The B3LYP/6-31G*-computed critical structures of all selected $\mathbf{I_X}$ ions are given in Table S1 of the Supporting Information. Only a single zero-order critical structure has been identified on the $\mathbf{I_F}$,[10] $\mathbf{I_{Si}}$,[10] $\mathbf{I_{Ge}}$, and $\mathbf{I_{Sn}}$ potential energy surfaces (PES), whose most significant geometrical parameters are given in Figure 1. In contrast, two zero-order critical structures have been found for the $\mathbf{I_X}$ ions (X = H, CN, Br, Cl, CH_3O, $COOCH_3$, CH_3, and C_6H_5). However, after ZPVE corrections, only one stable structure of $\mathbf{I_X}$ (X = CN, Br, Cl, and CH_3O) is found, corresponding to the $\mathbf{I^Z_X}$ conformer. The relevant geometries are shown in Figure 1. The resulting picture fully conforms to the electrostatic field and hyperconjugative effects of the substituent at C5. Thus, σ-electron-donor substituents (X = $CH_3)_3Si$, $CH_3)_3Ge$, and $CH_3)_3Sn$) favor the $\mathbf{I^E_X}$ invertomer, whereas those with strong σ-electron-withdrawing character (X = F, Br, Cl, CH_3O, CN, $COOCH_3$, and C_6H_5) favor the $\mathbf{I^Z_X}$ one. Among these, those with less pronounced σ-electron-withdrawing properties, i.e., $COOCH_3$ and C_6H_5, exhibit two zero-order critical structures even after ZPVE corrections.

The 298 K C−O bond enthalpies of $\mathbf{II^Z_{Me}}$ and $\mathbf{II^E_{Me}}$ and the 298 K $\mathbf{II^E_{Me}} \rightarrow \mathbf{II^Z_{Me}}$ epimerization enthalpy, calculated at the B3LYP/6-31G* level of theory, are listed in Table 1.

Radiolytic Experiments. Table 2 reports the absolute and relative yields of the ^{18}O-labeled ethers $\mathbf{2^E_{Me}}$ and $\mathbf{2^Z_{Me}}$ obtained from the *extra-* (i) and *intracomplex* (ii) pathways of Scheme 1. Table 2 reports average values obtained from several separate irradiations carried out under the same experimental conditions and whose reproducibility is expressed by the uncertainty level quoted. The ionic origin of ethers $\mathbf{2^E_{Me}}$ and $\mathbf{2^Z_{Me}}$ is demonstrated by the sharp decrease (over 85%) of their abundance as the $(C_2H_5)_3N$ concentration is quintupled.

TABLE 1. B3LYP/6-31G* Reaction Enthalpies.

reaction	ΔH_{298} (kcal mol^{-1})
$\mathbf{II^E_{Me}} \rightarrow \mathbf{II^Z_{Me}}$	−0.11
$\mathbf{II^E_{Me}} \rightarrow \mathbf{I^E_{Me}} + CH_3OH$	+11.05
$\mathbf{II^Z_{Me}} \rightarrow \mathbf{I^Z_{Me}} + CH_3OH$	+10.72

As already pointed out in a related paper,[10] the relative distribution of labeled ethers $\mathbf{2^Z_{Me}}$ and $\mathbf{2^E_{Me}}$ can be taken as representative of that of the corresponding ionic precursors $\mathbf{II^Z_{Me}}$ and $\mathbf{II^E_{Me}}$, if the efficiency of their neutralization by the strong base B = $(C_2H_5)_3N$ (proton affinity (PA) = 234.7 kcal mol^{-1})[20] is taken equal to unity. The rate constant ratio k_{syn}/k_{anti} of Scheme 1 can be expressed by the $[\mathbf{2^Z_{Me}}]/[\mathbf{2^E_{Me}}]$ ratio, once corrected by the extent of $\mathbf{II^Z_{Me}} \leftrightarrows \mathbf{II^E_{Me}}$ epimerization by the time τ of their neutralization with the strong base B ($\tau = (k_b[B])^{-1}$) at each temperature.[21]

This piece of information is obtained by generating directly the $\mathbf{II^Z_{Me}}$ and $\mathbf{II^E_{Me}}$ intermediates from the corresponding alcohols $\mathbf{3^Z_{Me}}$ or $\mathbf{3^E_{Me}}$ (route iii of Scheme 1) and by measuring their epimerisation rates ($k_{E\rightarrow Z}$ vs $k_{Z\rightarrow E}$) under conditions similar to those of Table 2. The yield factors of the unlabeled ethers $\mathbf{2^Z_{Me}}$ and $\mathbf{2^E_{Me}}$, obtained from route iii of Scheme 1, are reported in Table 3 under the ζ and ϵ headings, respectively.

The $k_{Z\rightarrow E}$ and $k_{E\rightarrow Z}$ rate constants can be expressed as in eqs 1 and 2, respectively, if $\mathbf{II^E_{Me}}$ epimerises by the ζ fraction and $\mathbf{II^Z_{Me}}$ by the ϵ fraction, during their lifetime τ:[10]

$$k_{Z\rightarrow E} = \frac{\epsilon_{eq}}{\tau} \ln\left(\frac{\epsilon_{eq}}{\epsilon_{eq} - \epsilon}\right), \text{ with } \epsilon_{eq} = \frac{K_{eq}}{1 + K_{eq}} \qquad (1)$$

and

$$k_{E\rightarrow Z} = \frac{\zeta_{eq}}{\tau} \ln\left[\frac{\zeta_{eq}}{\zeta_{eq} - \zeta}\right], \text{ with } \zeta_{eq} = \frac{1}{1 + K_{eq}} \qquad (2)$$

At each defined temperature and equal *B* concentrations, the $\mathbf{II^Z_{Me}} \leftrightarrows \mathbf{II^E_{Me}}$ equilibrium constant K_{eq} can be calculated as in eq 3.[10]

$$K_{eq} = \frac{\epsilon}{\zeta} \qquad (3)$$

Linear correlations are observed between the logarithm of $k_{E\rightarrow Z}$, $k_{Z\rightarrow E}$, and K_{eq} and the inverse of temperature (Figure 2). The relevant kinetic and thermodynamic parameters are reported in Table 4. According to these values, intermediate $\mathbf{II^Z_{Me}}$ is more stable than epimer $\mathbf{II^E_{Me}}$ by 1.2 ± 0.6 kcal mol^{-1}.

(19) Scott, A. P.; Radom, L. *J. Phys. Chem.* **1996**, *100*, 16502.

(20) Lias, S. G.; Hunter, E. P. L. *J. Phys. Chem. Ref. Data* **1998**, *27*, 413.

(21) The collision constant k_b between $\mathbf{II^Z_X}$ (or $\mathbf{II^E_X}$) and $(C_2H_5)_3N$ is calculated according to: Su, T.; Chesnavitch, W. J. *J. Chem. Phys.* **1982**, *76*, 5183.

TABLE 2. ^{18}O-Labeled Product Distribution from the Gas-Phase Attack of Gaseous Acids on $\mathbf{1_{Me}}$ in the Presence of $B{=}N(CH_3)_3$[a]

reaction path	$R^{18}OH$ (R, Torr)	B (Torr)	T (°C)	τ[b] ($\times 10^8$ s)	$[\mathbf{2^Z_{Me}}]$[c]	$[\mathbf{2^E_{Me}}]$[c]	absolute yield,[d] ($G_{(M)} \times 10^2$)
i	CH_3, 1.33	0.44	40	6.45	0.592	0.408	51.0
i	CH_3, 1.32	0.44	60	6.88	0.560	0.440	86.2
i	CH_3, 1.33	0.44	80	7.32	0.545	0.455	13.6
i	CH_3, 1.23	0.44	100	8.21	0.540	0.460	26.1
ii	H, 3.11	0.44	40	6.45	0.576	0.424	6.7
ii	H, 2.89	0.44	60	6.88	0.577	0.423	4.0
ii	H, 2.90	0.44	80	7.32	0.560	0.440	3.7
ii	H, 3.06	0.44	100	8.21	0.549	0.451	2.6

[a] Bulk gas, 750 Torr; $\mathbf{1_{Me}}$, 0.2−0.3 Torr; O_2, 4 Torr; radiation dose: 2×10^4 Gy (dose rate: 1×10^4 Gy h^{-1}). [b] Reaction time, τ, calculated from the reciprocal of the first-order collision constant between intermediates $\mathbf{II^E_{Me}}$ and $\mathbf{II^Z_{Me}}$ and B. [c] Each value is the average of several determinations, with an uncertainty level of ca. 10%. [d] $G_{(M)}$ as the number of molecules M produced per 100 eV of absorbed energy.

TABLE 3. Kinetics of Gas-Phase Epimerization of $\mathbf{II^E_{Me}}$ and $\mathbf{II^Z_{Me}}$ in the Presence of $B{=}N(CH_3)_3$[a]

substrate (Torr)	B (Torr)	T (°C)	τ ($\times 10^8$ s)[b]	ζ[c]	$k_{E\rightarrow Z}$ ($\times 10^{-6}$ s^{-1})[d]	K_{eq}[d]
$\mathbf{3^E_{Me}}$ (0.21)	0.466	40	6.056	0.1837	3.554 (6.551)	0.512 (−0.290)
$\mathbf{3^E_{Me}}$ (0.22)	0.488	60	6.174	0.2241	5.479 (6.739)	0.614 (−0.212)
$\mathbf{3^E_{Me}}$ (0.28)	0.428	80	7.487	0.2601	5.754 (6.760)	0.768 (−0.114)
$\mathbf{3^E_{Me}}$ (0.25)	0.469	100	7.241	0.3304	6.640 (6.822)	0.672 (−0.173)
substrate (Torr)	B (Torr)	T (°C)	τ ($\times 10^8$ s)[b]	ϵ[c]	$k_{Z\rightarrow E}$ ($\times 10^{-6}$ s^{-1})[d]	K_{eq}[d]
$\mathbf{3^Z_{Me}}$ (0.20)	0.466	40	6.056	0.0940	1.818 (6.260)	0.512 (−0.290)
$\mathbf{3^Z_{Me}}$ (0.24)	0.488	60	6.174	0.1375	2.938 (6.468)	0.614 (−0.212)
$\mathbf{3^Z_{Me}}$ (0.23)	0.428	80	7.487	0.1998	3.596 (6.556)	0.768 (−0.114)
$\mathbf{3^Z_{Me}}$ (0.27)	0.469	100	7.241	0.2220	4.462 (6.649)	0.672 (−0.173)

[a] CH_3Cl, 750 Torr; $H_2{}^{18}O$, 3 Torr; O_2, 6 Torr; radiation dose: 2×10^4 Gy (dose rate: 1×10^4 Gy h^{-1}). [b] Reaction time, τ, calculated from the reciprocal of the first-order collision constant between intermediates $\mathbf{II^E_{Me}}$ and $\mathbf{II^Z_{Me}}$ and B. [c] $\zeta = [\mathbf{2^Z_{Me}}]/([\mathbf{2^E_{Me}}] + [\mathbf{2^Z_{Me}}])$; $\epsilon = [\mathbf{2^E_{Me}}]/([\mathbf{2^E_{Me}}] + [\mathbf{2^Z_{Me}}])$. Each value is the average of several determinations, with an uncertainty level of ca. 5%. [d] See text; log k and log K_{eq} in parentheses.

TABLE 4. Kinetic and Thermodynamic Parameters for the Gas-Phase Epimerization of $\mathbf{II^E_{Me}}$ and $\mathbf{II^Z_{Me}}$

epimerization reaction	Arrhenius equation[a]	corr coeff r^2	$\Delta H^{\ddagger}$ (kcal mol^{-1})	$\Delta S^{\ddagger}$ (cal mol^{-1} K^{-1})
$\mathbf{II^E_{Me}} \rightarrow \mathbf{II^Z_{Me}}$	$\log k_{E\rightarrow Z} = (8.1 \pm 0.4) - (2.1 \pm 0.7)x$	0.841	1.6 ± 0.7	-23.5 ± 2.5
$\mathbf{II^Z_{Me}} \rightarrow \mathbf{II^E_{Me}}$	$\log k_{Z\rightarrow E} = (8.6 \pm 0.3) - (3.4 \pm 0.4)x$	0.968	2.8 ± 0.4	-21.0 ± 0.5
epimerization reaction	van't Hoff equation[a]	corr coeff r^2	$\Delta H°$ (kcal mol^{-1})	$\Delta S°$ (cal mol^{-1} K^{-1})
$\mathbf{II^E_{Me}} \leftrightarrows \mathbf{II^Z_{Me}}$	$\log K_{eq} = (0.6 \pm 0.4) - (1.2 \pm 0.6)x$	0.657	1.2 ± 0.6	$+2.6 \pm 2.2$

[a] $x = 1000/2.303RT$.

Considering the uncertainties associated with the experimental measurements and theoretical calculations (±2 kcal mol^{-1}), this experimental stability difference well agrees with the B3LYP/6-31G*-calculated one ($\Delta H°(\mathbf{II^E_{Me}}) - \Delta H°(\mathbf{II^Z_{Me}}) = +0.11$ kcal mol^{-1}) (Table 1).

Knowledge of the $\mathbf{II^Z_{Me}} \leftrightarrows \mathbf{II^E_{Me}}$ epimerization extent during the ion lifetime τ allows k_{syn}/k_{anti} of Scheme 1 to be expressed as follows[10]

$$\frac{k_{syn}}{k_{anti}} = \frac{[\mathbf{2^Z_{Me}}] - \zeta}{[\mathbf{2^E_{Me}}] - \epsilon} \qquad (4)$$

with the $[\mathbf{2^Z_{Me}}]$ and $[\mathbf{2^E_{Me}}]$ values as listed in Table 2 and the ϵ and ζ terms, as recalculated at $t = \tau$ of Table 2 using eqs 1 and 2, respectively. The logarithm of the so-calculated k_{syn}/k_{anti} ratios exhibits a linear dependence upon the inverse of temperature. That concerning the *extracomplex* pathway i is shown in Figure 3 by the open square symbols. Table 5 reports the relevant Arrhenius equations and activation parameters, as calculated from the transition-state theory equation.

According to the B3LYP/6-31G* estimates, the activation barriers for the $\mathbf{I^Z_X} \leftrightarrows \mathbf{I^E_X}$ (X = H, CH_3, C_6H_5, and $COOCH_3$; Table S1 of Supporting Information) interconversion are very small and comparable to thermal energies (RT) within the 40−100 °C range. It is therefore

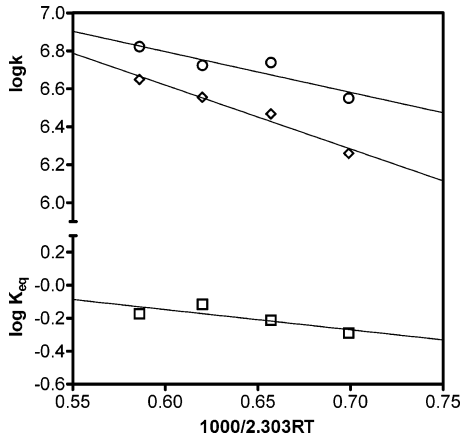

FIGURE 2. Temperature dependence of the $k_{E\rightarrow Z}$ (circles) and $k_{Z\rightarrow E}$ (diamonds) rates and of the relevant $K_{eq} = k_{Z\rightarrow E}/k_{E\rightarrow Z}$ (squares) concerning the gas-phase $\mathbf{II^Z_{Me}} \leftrightarrows \mathbf{II^E_{Me}}$ epimerization.

TABLE 5. Differential Arrhenius Parameters for the Formation of II^{E}_{Me} and II^{Z}_{Me} from the Gas-Phase Attack of $CH_3{}^{18}OH$ on I_{Me}

reaction path	Arrhenius equation[a]	corr coeff r^2	$\Delta\Delta H^{\ddagger}$ (kcal mol^{-1})	$\Delta\Delta S^{\ddagger}$ (cal mol^{-1} K^{-1})
i	$\log(k_{syn}/k_{anti}) = -(1.0 \pm 0.2) + (1.6 \pm 0.4)x$	0.905	-1.6 ± 0.4	-4.6 ± 0.8
ii	$\log(k_{syn}/k_{anti}) = -(0.5 \pm 0.2) + (0.9 \pm 0.3)x$	0.831	-0.9 ± 0.3	-2.5 ± 1.0

[a] $x = 1000/2.303RT$.

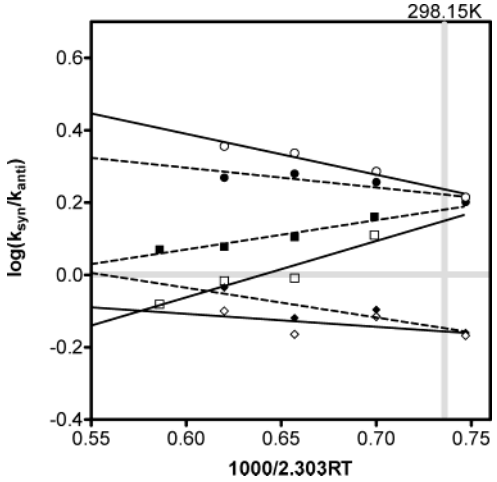

FIGURE 3. Temperature dependence of the uncorrected $[2^{Z}_{Me}]/[2^{E}_{Me}]$ (solid symbols) and the corresponding k_{syn}/k_{anti} terms (open symbols; eq 4) for the gas-phase reaction of $\mathbf{I_X}$ (X = F (circles), CH_3 (squares), and $(CH_3)_3Si$ (diamonds)) with methanol.

plausible that $\mathbf{I^{Z}_{Me}} \leftrightarrows \mathbf{I^{E}_{Me}}$ bridge-flipping is fast in the $[\mathbf{I_{Me}}\cdot CH_3{}^{18}OH]$ complex as well relative to its evolution to the corresponding addition products $\mathbf{II^{Z}_{Me}}$ and $\mathbf{II^{E}_{Me}}$.

In this frame, the schematic 298 K enthalpy and free energy profiles for the gas-phase *extracomplex* (i) and *intracomplex* (ii) addition of $CH_3{}^{18}OH$ to $\mathbf{I_{Me}}$ (profiles A) are shown in Figure 4 together with the profiles concerning the same reactions on $\mathbf{I_F}$ (profiles B) and $\mathbf{I_{Si}}$ (profiles C) reported previously.[10] Their comparison indicates the following: (i) irrespective of the specific reaction pathway, *syn* addition of $CH_3{}^{18}OH$ to $\mathbf{I_{Me}}$ is enthalpically favored over the competing *anti* attack (profiles A). The reverse is true for the attack of $CH_3{}^{18}OH$ on both $\mathbf{I_F}$ (profiles B) and $\mathbf{I_{Si}}$ ions (profiles C). (ii) Irrespective of the specific ion $\mathbf{I_X}$, its gas-phase reaction with $CH_3{}^{18}OH$ is characterized by adverse activation entropies increasing in the order $\mathbf{I_{Si}}$ (profiles C) < $\mathbf{I_F}$ (profiles B) < $\mathbf{I_{Me}}$ (profiles A). (iii) The adverse entropy contributions are more important in the extracomplex *syn* attack of $CH_3{}^{18}OH$ on $\mathbf{I_{Me}}$ than in the *intracomplex* one (profiles A). The reverse is true in the *anti* attack of $CH_3{}^{18}OH$ on $\mathbf{I_F}$ (profiles B). (4) Owing to significant differences in the adverse activation entropies, gas-phase facial selectivity of ions $\mathbf{I_X}$ (X = CH_3, F, and $(CH_3)_3Si$) depends markedly on both the reaction temperature and the nature of the ionic reactant. Thus, as shown by the full lines of Figure 3, $k_{syn}/k_{anti} > 1$ for $\mathbf{I_F}$ and increases with T. In contrast, $k_{syn}/k_{anti} < 1$ for $\mathbf{I_{Si}}$ and decreases by increasing T. Finally, $k_{syn}/k_{anti} > 1$ for $\mathbf{I_{Me}}$ below T = 69 °C and becomes $k_{syn}/k_{anti} < 1$ above that temperature.

The broken lines of Figure 3 refer to the T dependence of the phenomenological $\log([2^{Z}_{X}]/[2^{E}_{X}])$ values for $\mathbf{I_X}$ (X = CH_3, F, and $(CH_3)_3Si$), uncorrected for the $\mathbf{II^{Z}_{X}} \leftrightarrows \mathbf{II^{E}_{X}}$ epimerization extent during the ion lifetime τ. If compared to the corresponding full lines of Figure 3, one can realize that, at 298.15 K, the deviation of the uncorrected $[2^{Z}_{X}]/[2^{E}_{X}]$ ratios from the corresponding k_{syn}/k_{anti} values does not exceed 7.3% for $\mathbf{I_X}$ (X = CH_3) and is much smaller for $\mathbf{I_X}$ (X = F and $(CH_3)_3Si$). Given the opposite electronic properties of the Me, F, and Me_3Si substituents, it is plausible to extend the correspondence between the uncorrected $[2^{Z}_{X}]/[2^{E}_{X}]$ ratio and the actual diastereoselectivity term k_{syn}/k_{anti} to all selected $\mathbf{I_X}$ ions.

TABLE 6. Facial Selectivity of I_X at 25 °C

substituent (X)	$([2^{Z}_{X}]/[2^{E}_{X}])_{gas\ phase}$ extracomplex path (i)	$([2^{Z}_{X}]/[2^{E}_{X}])_{gas\ phase}$ intracomplex path (ii)	$([4^{Z}_{X}]/[4^{E}_{X}])_{solution}$[a] CH_2Cl_2	$([4^{Z}_{X}]/[4^{E}_{X}])_{solution}$[a] CH_3NO_2
CN	1.48	n.d.[b]	6.70	7.33[c]
F	1.55	2.71	9.00	very large
Cl	2.98	7.57	4.88	32.33
Br	2.16	5.89	3.55	4.88
OCH_3	2.43	2.40	6.14	5.67
$COOCH_3$	3.79	3.71	2.57	2.85
C_6H_5	2.37	3.24	1.86	1.94
CH_3	1.29	1.57	1.56	1.27
$(CH_3)_3Si$	0.70	0.58	0.54	1.00
$(CH_3)_3Sn$	0.65	n.d.	n.d.	n.d.

[a] References 4 and 6. [b] n.d. = no reaction. [c] This study, X = CN, Z/E = 88/12.

In their *extra*- (i) and *intracomplex* (ii) addition to $CH_3{}^{18}OH$, the $\mathbf{I_F}$ and $\mathbf{I_{CN}}$ ions display a $\log([2^{Z}_{X}]/[2^{E}_{X}])$ vs T^{-1} linear dependence with a negative slope (see Figures S1−S6 in Supporting Information), indicating that their reaction with methanol obeys the same B-like energy profile (Figure 4). In the same way, the $\mathbf{I_X}$ (X = Br, Cl, CH_3O, CH_3, $COOCH_3$, and C_6H_5) ions exhibit $\log([2^{Z}_{X}]/[2^{E}_{X}])$ vs T^{-1} linear curves with positive slopes (see Figures S1−S6 in Supporting Information), thus suggesting that their addition to methanol is governed by the same A-like energy profile (Figure 4). The $[2^{Z}_{X}]/[2^{E}_{X}]$ values from the gas-phase *extra*- (i) and *intracomplex* (ii) addition of $CH_3{}^{18}OH$ to $\mathbf{I_X}$, evaluated at 25 °C from the relevant Arrhenius plots, are given in Table 6. These values are compared in Table 6 with the relative Z/E distribution of the 2-methyl-2-chloro-5-X-adamantanes (4^{Z}_{X} and 4^{E}_{X}, respectively) produced from the attack of HCl to $\mathbf{1_X}$ in either CH_2Cl_2 or CH_3NO_2 at 25 °C.[2,4]

Discussion

Energy Profiles and Transition Structures. The selectivity data of the two first columns of Table 6 are plotted in Figure 5. The unity slope (0.96 ± 0.20; r^2 = 0.878) of the full line points to equal selectivity for the *intracomplex* (ii) vs the *extracomplex* (i) path for $\mathbf{I_X}$ (X = H, CH_3O, CH_3, $COOCH_3$, and C_6H_5). In contrast, the broken line in the same Figure (slope: 3.21 ± 0.39; r^2 = 0.972) indicates that the gas-phase *intracomplex* path (ii) is much more selective than the *extracomplex* (i) one for $\mathbf{I_X}$ (X = $(CH_3)_3Si$, F, Cl, and Br). The origin for these

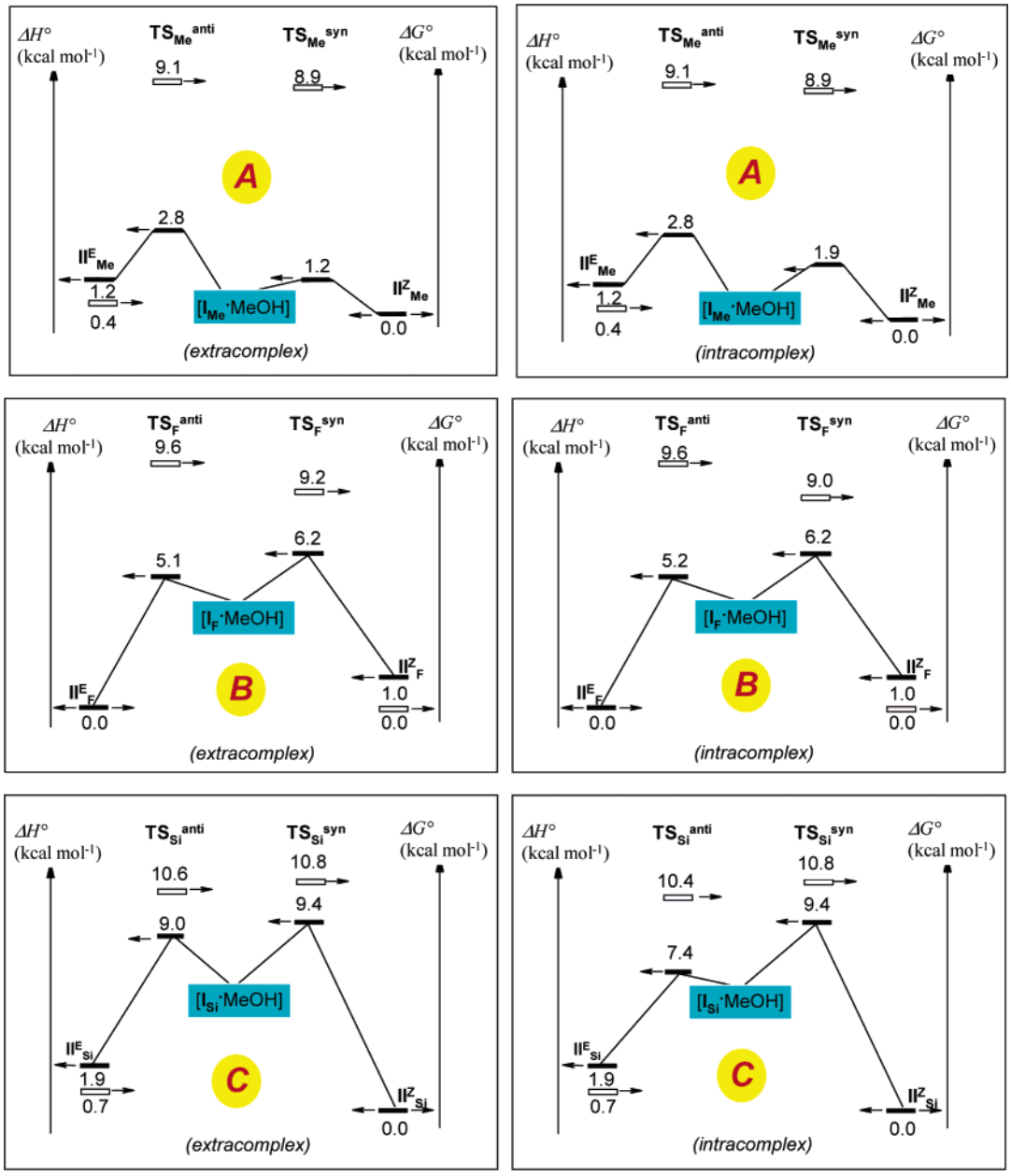

FIGURE 4. 298.15 K enthalpy (solid bars) and free energy (open bars) profiles of the gas-phase reaction (i) and (ii) between $\mathbf{I_X}$ (X = CH_3 (profiles A), F (profiles B), and $(CH_3)_3Si$ (profiles C)) and methanol.

differences can be appreciated by inspecting Figure 4. Indeed, profiles A of Figure 4 show that the enthalpy barrier for the *intracomplex syn* addition (ii) of $CH_3{}^{18}OH$ to $\mathbf{I_{Me}}$ is 0.7 kcal mol^{-1} higher than that of the corresponding *extracomplex* reaction i. No significant differences between the corresponding free-energy profiles are observed at 298 K. Almost identical enthalpy profiles B are associated with the *extra-* (i) and *intracomplex* (ii) addition of $CH_3{}^{18}OH$ to $\mathbf{I_F}$. However, at 298 K, the different entropy contributions make the *syn* vs *anti* free energy difference 0.2 kcal mol^{-1} larger in path ii than in path i. Finally, profiles C of Figure 4 show that the enthalpy barrier of the *extracomplex anti* addition i is 1.6 kcal mol^{-1} higher than that of the *intracomplex* path ii. Most of the activation enthalpy differences are wiped off by the activation entropy contributions which make the *syn* vs *anti* free energy difference 0.2 kcal mol^{-1} larger in path ii than in path i at 298 K. Thus, a subtle interplay between activation enthalpy and entropy factors makes the *intracomplex* $CH_3{}^{18}OH$ addition (ii) on $\mathbf{I_F}$ and $\mathbf{I_{Si}}$ more selective than the *extracomplex* one (i) (broken line in Figure 5), while the two processes are almost equally selective with $\mathbf{I_{Me}}$ (full line in Figure 5).

The experimental activation enthalpies of the gas-phase attack of $CH_3{}^{18}OH$ on $\mathbf{I_{Me}}$ (profiles A of Figure 4) amount to only one-fourth or even less of the B3LYP/6-31G* C−O bond dissociation energies of oxonium ions $\mathbf{II^Z_{Me}}$ and $\mathbf{II^E_{Me}}$ (Table 1). These moderate activation enthalpies, coupled with the large adverse activation entropies, point to the [$\mathbf{I_{Me}}$·$CH_3{}^{18}OH$] encounter complexes from paths i and ii as evolving to their products through tight transition structures $\mathbf{TS_{Me}}^{anti}$ and $\mathbf{TS_{Me}}^{syn}$ characterized by a large degree of C−O bonding. Some information about these transition structures may arise

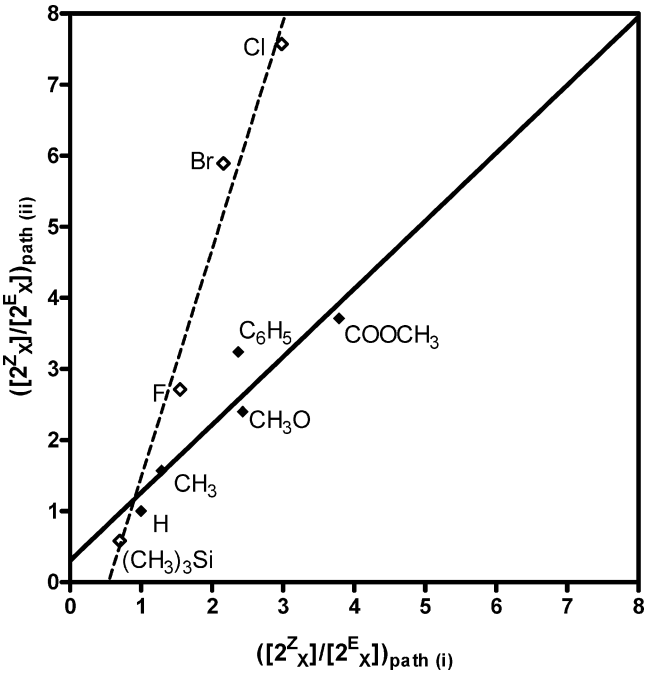

FIGURE 5. Plot of the $[2^Z_X]/[2^E_X]$ ratios from the gas-phase *intracomplex* vs *extracomplex* attack of methanol on $\mathbf{I_X}$ at 25 °C.

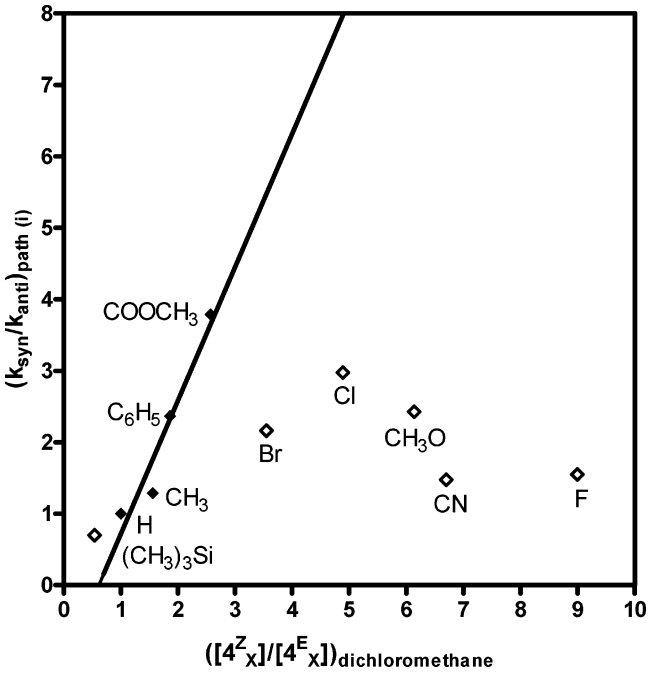

FIGURE 6. Plot of the $[2^Z_X]/[2^E_X]$ ratio from the gas-phase *extracomplex* attack of methanol on $\mathbf{I_X}$ versus the $[4^Z_X]/[4^E_X]$ product ratio from the chloride ion attack to $\mathbf{I_X}$ in CH_2Cl_2 at 25 °C.

from a comparison of the 298 K free energy profiles in Figure 4. At 298 K, $\mathbf{I_{Me}}$ is almost as reactive as $\mathbf{I_F}$ toward $CH_3{}^{18}OH$, although the relevant activation enthalpy and entropy terms are considerably different. These differences can find a plausible explanation in the structural flexibility of $\mathbf{I_{Me}}$ ($\mathbf{I^Z_{Me}} \leftrightarrows \mathbf{I^E_{Me}}$) as compared to the rigidity of the only stable *Z* conformer of $\mathbf{I_F}$ ($\mathbf{I^Z_F}$). The small activation enthalpies and the large adverse activation entropies[22] associated with $\mathbf{TS_{Me}}^{anti}$ and $\mathbf{TS_{Me}}^{syn}$ (A in Figure 4) are consistent with a rapid $\mathbf{I^Z_{Me}} \leftrightarrows \mathbf{I^E_{Me}}$ interconversion which allows facial discrimination by the $CH_3{}^{18}OH$ nucleophile only when strictly bound to the C2 center.[23] Contrary to $\mathbf{I_{Me}}$, only the rigid $\mathbf{I^Z_F}$ and $\mathbf{I^E_{Si}}$ structures have been identified on the relevant B3LYP/6-31G*-computed potential energy surface. The large activation enthalpies and small adverse activation entropies associated with $\mathbf{TS_X}^{anti}$ and $\mathbf{TS_X}^{syn}$ (X = F and $(CH_3)_3Si$, B and C in Figure 4) are consistent with a $CH_3{}^{18}OH$ nucleophile which does not need to be so close to the C2 center of the ion to discriminate between its faces. Long-range H-bonding may be sufficient to drive the nucleophile on the asymmetric faces of the rigid ion. This view may explain also the more pronounced selectivity of the *intracomplex* path (ii) vs the *extracomplex* (i) one, observed for $\mathbf{I_X}$ (X = $(CH_3)_3Si$, F, Cl, and Br; Figure 5). In the *intracomplex* path ii, the incipient $CH_3{}^{18}OH$ nucleophile *is necessarily originated as H-bonded* to the CH_3 hydrogens of the putative $\mathbf{I_X}$ ion. In other words, it is generated on a specific acidic site of the ion and relatively close to it. On the contrary, in the *extracomplex* path i, the external $CH_3{}^{18}OH$ nucleophile can preliminary interact with all other acidic hydrogens of the $\mathbf{I_X}$ ion, including those at the CH_3 group.[23] In this case, facial discrimination by the nucleophile may take place when more removed from the C2 reaction site. Thus, the 3.21 ± 0.39 slope of the broken line of Figure 5 reflects the different position of the relatively loose $\mathbf{TS_X}^{anti}$ and $\mathbf{TS_X}^{syn}$ (X = $(CH_3)_3Si$, F, Cl, and Br) along the reaction coordinates of the two processes i and ii. The marked tightness of $\mathbf{TS_X}^{anti}$ and $\mathbf{TS_X}^{syn}$ (X = H, CH_3O, CH_3, $COOCH_3$, and C_6H_5) makes such difference vanishingly small, as demonstrated by the unity slope of the full line of Figure 5.

The Origin of the Diastereofacial Selectivity in the Gas Phase and in Solution. The origin of the gas-phase facial selectivity of $\mathbf{I_{Me}}$ and $\mathbf{I_F}$ toward methanol can be found in the frame of Leffler−Hammond postulate[24,25] by assuming that the stability difference of $\mathbf{TS_X}^{anti}$ vs $\mathbf{TS_X}^{syn}$ somewhat reflects that of the $\mathbf{II^E_X}$ vs $\mathbf{II^Z_X}$ products (profiles A and B of Figure 4).[10] This indicated that the σ-hyperconjugative effects of the substituent which control the relative stability of the $\mathbf{I^E_X}$ vs $\mathbf{I^Z_X}$ conformers do influence also that of their reaction products and the corresponding transition structures. As pointed out before,[10] the large difference in the adverse entropies associated with $\mathbf{TS_X}^{anti}$ and $\mathbf{TS_X}^{syn}$ (Figure 4) is due to their position along the reaction coordinate and reflect the different physical space available to the $CH_3{}^{18}OH$ nucleophile in its approach to the *zu* and *en* asymmetric faces of the distorted $\mathbf{I_X}$ ions.

The gas-phase facial selectivities of $\mathbf{I_X}$ ion in the *extracomplex* pathway (i) at 25 °C (Table 6) are plotted in Figure 6 against the *Z*/*E* distribution of the 2-methyl-2-chloro-5-X-adamantanes ($\mathbf{4^Z_X}$ and $\mathbf{4^E_X}$, respectively) generated in CH_2Cl_2 (ϵ = 8.9) at 25 °C from the chloride ion addition to $\mathbf{I_X}$.[2,4] A linear correlation (slope: 1.87 ±

(22) A contribution to the adverse activation entropies may arise from torsional freezing of the $\mathbf{I_X}$ moiety in $\mathbf{TS_X}$.
(23) Filippi, A. *Chem. Eur. J.* **2003**, *9*, 5396.
(24) Leffler, J. E. *Science* **1953**, *117*, 340.
(25) Hammond, G. S. *J. Am. Chem. Soc.* **1955**, *77*, 334.

0.36; $r^2 = 0.932$) can be drawn for ions, such as $\mathbf{I_X}$ (X = H, CH_3, $COOCH_3$, and C_6H_5), which establish a $\mathbf{I^Z_X} \leftrightarrows \mathbf{I^E_X}$ conformational equilibrium in the gas phase. Large negative deviations from linearity are instead observed for ions $\mathbf{I^Z_X}$ (X = CN, Br, Cl, CH_3O, and F) stable in the gas phase only in the *Z* conformation (Figure 1). A similar plot can be obtained by comparing the same gas-phase $\mathbf{I_X}$ diastereoselectivities with the calculated polar-field induced facial selectivity of $\mathbf{I_X}$ toward Cl^- in CH_2Cl_2 (see Figure S7 in the Supporting Information).[2,4] A linear correlation (slope = 0.90 ± 0.04; $r^2 = 0.996$) is indeed observed for $\mathbf{I_X}$ (X = H, CH_3, $COOCH_3$, and C_6H_5), while ions $\mathbf{I_X}$ (X = CN, Br, Cl, CH_3O, and F) exhibit large negative deviations.

The above linear correlations indicate that the factors which control the facial selectivity of $\mathbf{I_X}$ toward Cl^- in CH_2Cl_2 are also operative in the gas-phase pathway i. This conclusion is valid for ions with X = H, CH_3, $COOCH_3$, and C_6H_5, i.e., substituents favoring the occurrence of a rapid $\mathbf{I^Z_X} \leftrightarrows \mathbf{I^E_X}$ conformational equilibrium in both the gas phase and in CH_2Cl_2 solutions (vide infra).[26]

The large deviation from linearity of $\mathbf{I_X}$ (X = CN, Br, Cl, CH_3O, and F) (Figure 6) may find a plausible rationale in the specific ion solvation in CH_2Cl_2. The presence of the strong electron-withdrawing X group in these ions favors positive charge localization at the C2 center, and hence, its solvation and ion pairing in solution. While these ions are found to be stable in the gas phase only in the *Z* conformation, ion solvation could in principle affect the relative stability of the $\mathbf{I^E_X}$ and $\mathbf{I^Z_X}$ forms so as to let them coexist in solution like $\mathbf{I_X}$ (X = H, CH_3, $COOCH_3$, and C_6H_5). This hypothesis complies with the observation that most of the $\mathbf{I_X}$ ions (except those with X = CH_3O and F) fits into a fairly good linear correlation (slope: 0.30 ± 0.03; $r^2 = 0.942$) between the measured $[\mathbf{4^Z_X}]/[\mathbf{4^E_X}]$ product distribution from chloride ion addition in CH_2Cl_2 at 25 °C and that calculated from the polar substituent parameters σ_F under the same conditions (see Figure S8 in the Supporting Information).[2,4] However, if solvent has no effects other than that of allowing the coexistence of both $\mathbf{I^Z_X}$ and $\mathbf{I^E_X}$ (X = CN, Br, Cl, CH_3O, and F), increasing the polarity of the solvent from CH_2Cl_2 (ϵ = 8.9) to CH_3NO_2 (ϵ = 37.5) would result in a marked reduction of their diastereoselectivity[27] relative to gas phase, in contrast with the experimental evidence (Table 6).

Perhaps a more convincing explanation for the large negative deviations from linearity, observed in Figure 6, can be found in the existence of a unique conformer ($\mathbf{I^Z_X}$; X = CN, Br, Cl, CH_3O, and F) not only in the gas phase but also in liquid CH_2Cl_2. In the gas phase, the adverse activation entropies associated with $\mathbf{TS_X}^{anti}$ and $\mathbf{TS_X}^{syn}$ are attributed to the different physical spaces available

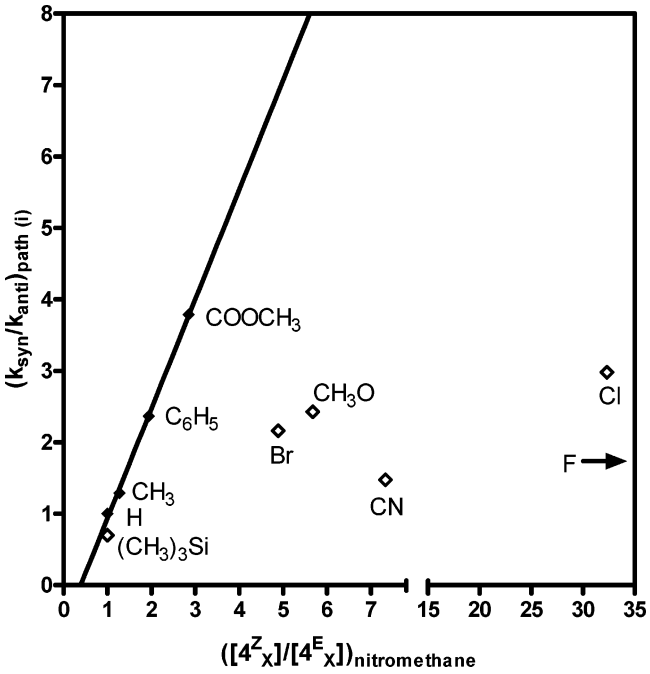

FIGURE 7. Plot of the $[\mathbf{2^Z_X}]/[\mathbf{2^E_X}]$ ratio from the gas-phase *extracomplex* attack of methanol on $\mathbf{I_X}$ versus the $[\mathbf{4^Z_X}]/[\mathbf{4^E_X}]$ product ratio from the chloride ion attack to $\mathbf{I_X}$ in CH_3NO_2 at 25 °C.

to the $CH_3{}^{18}OH$ nucleophile during its approach to the *zu* and *en* faces of the distorted $\mathbf{I^Z_X}$ structure (Figure 1).[10] In CH_2Cl_2, these spaces are partially occupied by solvent molecules whose local viscosity and dielectricity depend on their more or less organized arrangement over the asymmetric $\mathbf{I^Z_X}$ faces (the "differential face solvation" model). This implies that, relative to gas phase, not only the stability of the $\mathbf{TS_{Me}}^{anti}/\mathbf{TS_{Me}}^{syn}$ pair but also their position along the reaction coordinate may be profoundly modified by facial $\mathbf{I^Z_X}$ solvation.

The occurrence of rapid $\mathbf{I^Z_X} \leftrightarrows \mathbf{I^E_X}$ (X = H, CH_3, $COOCH_3$, and C_6H_5) conformational equilibria in liquid CH_2Cl_2[26] hampers any orderly assembling of solvent molecules over the two faces of the ion. Hence, differential facial solvation plays a minor role in these ions. As a consequence, a strict correlation exists between the gas-phase diastereoselectivity and that observed in CH_2Cl_2 solution (Figure 6) since it is controlled exclusively by double σ-hyperconjugation of the substituent with the reaction center. The lower diastereoselectivity, measured in CH_2Cl_2, is attributed to the effects of the viscosity and dielectricity of CH_2Cl_2 in determining the position of the $\mathbf{TS_X}^{anti}$ and $\mathbf{TS_X}^{syn}$ addition structures along the relevant reaction coordinates.

The same model applies to the chloride ion addition to $\mathbf{I_X}$ in CH_3NO_2,[2,4] as demonstrated the good linear correlation ($r^2 = 0.998$) between the gas-phase facial selectivities of $\mathbf{I^Z_X} \leftrightarrows \mathbf{I^E_X}$ (X = H, CH_3, $COOCH_3$, and C_6H_5) ions from the *extracomplex* pathway i and the $\mathbf{4^Z_X}$ vs $\mathbf{4^E_X}$ product distribution from the chloride ion attack to $\mathbf{I_X}$ in CH_3NO_2 (Figure 7).[2,4] A slope of 1.53 ± 0.05 is measured from the linear curve which well compares with that observed for the same ions in Figure 6 (slope: 1.87 ± 0.36). This correspondence further corroborates the hypothesis of a rapid conformational equilibrium of $\mathbf{I_X}$ (X = H, CH_3, $COOCH_3$, and C_6H_5) in the condensed phase,

(26) For $\mathbf{I^Z_X} \leftrightarrows \mathbf{I^E_X}$ (X = Me), see: (a) Finne, E. S.; Gunn, J. R.; Sorensen, T. S. *J. Am. Chem. Soc.* **1987**, *109*, 7816. (b) Dutler, R.; Rauk, A.; Sorensen, T. S.; Whitworth, S. M. *J. Am. Chem. Soc.* **1989**, *111*, 9024. (c) Buffam, D. J.; Sorensen, T. S.; Whitworth, S. M. *Can. J. Chem.* **1990**, *68*, 1889. (d) Martin, H. D.; Mayer, B. *Angew. Chem., Int. Ed. Engl.* **1983**, *22*, 283 and references therein.

(27) A reduction of facial selectivity in polar solvents can be attributed to a decrease in the $\mathbf{I^Z_X}$ vs $\mathbf{I^E_X}$ stability gap by specific ion solvation (ion polarity effect) as well as by an attenuation of the polar field effect of the X substituent on the $\mathbf{I^Z_X} \leftrightarrows \mathbf{I^E_X}$ equilibrium (dielectric constant effect).

whose facial selectivity is essentially independent of the specific reaction medium used, whether CH_2Cl_2 or CH_3NO_2.

Instead, the reaction environment dramatically affects the diastereoselectivity of those ions $\mathbf{I^Z_X}$ (X = CN, Br, Cl, CH_3O, and F) present in a single conformation both in the gaseous and condensed phase (Table 6). These systems exhibit a much larger selectivity in CH_3NO_2 than in CH_2Cl_2. This difference fits into the "differential face solvation" model and can be attributed to the specific assembling of the solvent molecules (including the counterion) around the two asymmetric faces of the distorted $\mathbf{I^Z_X}$ structure.

The same conclusions are reached when comparing the diastereofacial selectivity of the same $\mathbf{I_X}$ ions in their gas phase *intracomplex* (ii) addition to $CH_3{}^{18}OH$ with that measured at 298 K in the attack of HCl to $\mathbf{1_X}$ in CH_2Cl_2 and CH_3NO_2 (see Figures S9 and S10 in Supporting Information, respectively).[2,4] A fairly good linear correlation ($r^2 = 0.866$) is observed for the $\mathbf{I^Z_X} \leftrightarrows \mathbf{I^E_X}$ (X = H, CH_3, $COOCH_3$, and C_6H_5) ions in CH_2Cl_2. Its slope (1.85 ± 0.52) is comparable to that measured for the same reactions in CH_3NO_2 (1.50 ± 0.35; $r^2 = 0.900$).

The good statistics ($r^2 = 0.932$; $r^2 = 0.998$) attached to the linear correlations of Figures 6 and 7, respectively, are consistent with the dynamic view of the nucleophile exploring, both in the gas-phase *extracomplex* path (i) and in solution, the entire physical space over the *zu* and *en* faces of the $\mathbf{I_X}$ (X = H, CH_3, $COOCH_3$, and C_6H_5) ions without any predetermined interaction with a specific $\mathbf{I_x}$ center. In contrast, the much worse statistics observed when the $\mathbf{I_X}$ (X = H, CH_3, $COOCH_3$, and C_6H_5) diastereoselectivity from the gas-phase *intracomplex* path (ii) is plotted against that measured in either CH_2Cl_2 ($r^2 = 0.866$; Figure S9 in the Supporting Information) or CH_3NO_2 ($r^2 = 0.900$; Figure S10 in the Supporting Information) can be the result of a different dynamics in the nucleophilic addition. Indeed, in the gas-phase *intracomplex* path (ii), the incipient nucleophile ($CH_3{}^{18}OH$) can attack the C2 center while still interacting with the CH_3 hydrogens of the putative $\mathbf{I_X}$ ion. A similar specific interaction can be efficiently superseded in solution by ion/counterion solvation.

Conclusions. The gas-phase diastereofacial selectivity of 2-methyl-5-X-adamant-2-yl cations $\mathbf{I_X}$ (X = CN, Cl, Br, F, CH_3O, $COOCH_3$, C_6H_5, CH_3, $(CH_3)_3Si$, and $(CH_3)_3Sn$) toward methanol is mainly controlled by double-σ-hyperconjugative effects of the X substituent. These effects manifest themselves by generating two different scenarios. Thus, the facial selectivity of $\mathbf{I_X}$ (X = σ-electron-donor) responds to the difference in the relevant activation enthalpies with minor, comparable adverse entropy contributions. In contrast, the facial selectivity of $\mathbf{I_X}$ (X = σ-electron-acceptor) is mainly controlled by adverse entropy contributions which are sufficiently different to moderate or even to outbalance the gap between the corresponding activation enthalpies in the 40−120 °C range. These scenarios reflect the effects of double σ-hyperconjugation on all the species involved in the reaction, including the distorted *syn* and *anti* conformers of $\mathbf{I_X}$, their $CH_3{}^{18}OH$ addition products, and the corresponding transition structures. Furthermore, σ-hyperconjugation determines the tight or loose character of the *syn* and *anti* transition structures and the magnitude of the corresponding activation entropy.

The gas-phase diastereofacial selectivity of $\mathbf{I_X}$ (X = H, $COOCH_3$, C_6H_5, and CH_3) correlates well with that measured for the same systems in solution. These ions establish a rapid $\mathbf{I^Z_X} \leftrightarrows \mathbf{I^E_X}$ conformational equilibrium in both media which, in the condensed phase, prevents any orderly assembling of the solvent molecules. In the lack of any differential disposition of the solvent molecules around the $\mathbf{I_X}$ faces, double σ-hyperconjugation of the substituent with the reaction center remains the only major factor determining the diastereoselectivity of these ions which, therefore, behave similarly in both the gas phase and in solution. The nucleophile discriminates between the two faces of $\mathbf{I_X}$ (X = H, $COOCH_3$, C_6H_5, and CH_3) only when very close to their charged C2 site. As a consequence, the reaction involves tight $\mathbf{TS_X}^{anti}$ and $\mathbf{TS_X}^{syn}$ transition structures and is characterized by limited activation enthalpies and large adverse activation entropies. Large deviations from gas-phase vs solution selectivity correlations are instead observed for those $\mathbf{I_X}$ (X = CN, Cl, Br, F, and OCH_3) ions which appears to be stable only in the *Z* conformation (i.e., $\mathbf{I^Z_X}$). These discrepancies are explained in terms of the "differential face solvation" model, related to local physical environment encountered by the nucleophile during its approach to the asymmetric *zu* and *en* faces of the distorted $\mathbf{I^Z_X}$ ion. Finally, it is significant to note that the preferential *syn*-face selectivity observed for $\mathbf{I_{Me}}$ in the gas phase from this study appears to resolve the long standing question[1b,28,29] regarding the relative intrinsic electron-donating ability of C−C and C−H bonds in unstrained saturated systems. Clearly, the former is σ-electron-withdrawing relative to the latter.

Acknowledgment. This work was supported by the Italian Ministero della Università e della Ricerca Scientifica e Tecnologica (MURST) and the Italian Consiglio Nazionale delle Ricerche (CNR) of Italy; the Australian Research Council; and the Canadian Natural Sciences and Engineering Research Council (NSERC).

Supporting Information Available: B3LYP/6-31G*-computed total energies of 2-methyl-5-X-adamant-2-yl cation $\mathbf{I_X}$. Observed and calculated ^{13}C NMR chemical shift data of the tertiary ethers $\mathbf{2^Z_X}$ and $\mathbf{2^E_X}$ (X = H, F, Cl, Br, $COOCH_3$, CH_3O, C_6H_5, CH_3, $(CH_3)_3Si$, and $(CH_3)_3Sn$). Temperature dependence of the facial selectivity measured in the gas-phase *extra-* and *intracomplex* addition of methanol to $\mathbf{I_X}$ (X = H, F, Cl, Br, $COOCH_3$, CH_3O, C_6H_5, CH_3, $(CH_3)_3Si$, and $(CH_3)_3Sn$). Plots of the experimental diastereoselectivity of $\mathbf{I_X}$ toward nucleophiles vs that calculated from polar-field substituent parameters. Plots of the $\mathbf{I_X}$ facial selectivity measured in the gas-phase *intracomplex* addition (ii) of methanol vs the Z/E distribution of the 2-methyl-2-chloro-5-X-adamantanes generated in the condensed-phase addition of the chloride ion addition to $\mathbf{I_X}$. This material is available free of charge via the Internet at http://pubs.acs.org.

JO049481L

(28) Cieplak, A. S. *Chem. Rev.* **1999**, *99*, 1265 and references therein.
(29) Rablen, P. R.; Hoffmann, R. W.; Hrovat, D. A.; Borden, W. T. *J. Chem. Soc., Perkin Trans. 2* **1999**, 1719 and references therein.